Link between Indian monsoon rainfall and physical erosion in the Himalayan system during the Holocene

Ronan Joussain, Zhifei Liu, Christophe Colin, Stéphanie Duchamp-Alphonse, Zhaojie Yu, Eva Moreno, Léa Fournier, Sébastien Zaragosi, Arnaud Dapoigny, Laure Meynadier, et al.

AGU PUBLICATIONS

Geochemistry, Geophysics, Geosystems

RESEARCH ARTICLE
10.1002/2016GC006762

Link between Indian monsoon rainfall and physical erosion in the Himalayan system during the Holocene

Ronan Joussain[1,2], Zhifei Liu[2], Christophe Colin[1], Stéphanie Duchamp-Alphonse[1], Zhaojie Yu[1], Eva Moréno[3], Léa Fournier[4], Sébastien Zaragosi[4], Arnaud Dapoigny[5], Laure Meynadier[6], and Franck Bassinot[5]

[1]Laboratoire GEOsciences Paris-Sud, UMR 8148, CNRS-Université de Paris-Sud, Université Paris-Saclay, Orsay Cedex, France, [2]State Key Laboratory of Marine Geology, Tongji University, Shanghai, China, [3]Muséum National d'Histoire Naturelle, UMR 7207, Paris Cedex 05, France, [4]UMR CNRS 5805 EPOC, Université de Bordeaux, Pessac Cedex, France, [5]Laboratoire des Sciences du Climat et de l'Environnement, LSCE/IPSL, CEA-CNRS-UVSQ, Université Paris-Saclay, Gif-sur-Yvette, France, [6]Equipe de Géochimie et Cosmochimie, Institut de Physique du Globe de Paris -- Sorbonne Paris Cité, UMR 7154, Université Paris Diderot, Paris, France

Key Points:
- Sedimentary sources and weathering state of detrital material derived from the G-B river system over the last ~9.8 ka
- Increasing input of detrital material from the highlands (reliefs) during the early-middle Holocene
- Rapid response of erosion and sediment transfer of the G-B river system to changes in the dynamic of the summer monsoon rainfall

Supporting Information:
- Supporting Information S1
- Table S1
- Table S2

Correspondence to:
R. Joussain,
ronan.joussain@gmail.com

Citation:
Joussain, R., et al. (2017), Link between Indian monsoon rainfall and physical erosion in the Himalayan system during the Holocene, *Geochem. Geophys. Geosyst.*, *18*, 3452–3469, doi:10.1002/2016GC006762.

Received 5 DEC 2016
Accepted 6 JUL 2017
Accepted article online 21 JUL 2017
Published online 15 SEP 2017

Abstract Mineralogical and geochemical analyses conducted on cores located on the active channel-levee system of the northern Bengal Fan are used to establish changes in the weathering pattern and the sediment transport of the Himalayan system, and evaluate the effect of Indian summer monsoon rainfall during the Holocene. Our data indicate that during the Holocene, sediments from the northern Bengal Fan originate mainly from the G-B river system without any significant changes in the relative contribution of these rivers. From 9.8 to around 6 ka, relatively low smectite/(illite+chlorite) ratios and relatively high K/Si* ratios indicate high physical denudation rates of the Himalayan highlands together with a rapid transfer of the detrital material to the Bengal Fan. The period between 9.2 and 7 ka is associated to lower values of K/Si* and corresponds to the maximum of Indian monsoon rainfall which indicates a more important chemical weathering material that rapidly transits by the G-B river system without a long storage in the Indo-Gangetic plain. From 6.0 ka to present day, higher smectite/(illite+chlorite) ratio and lower K/Si* ratio document a gradual increase of sediments originated from the Indo-Gangetic plain, characterized by higher degree of chemical weathering. During the last 2.5 ka, the drastic increase in the smectite/(illite+chlorite) ratio could be associated to enhanced alteration of the plain soils due to anthropogenic activity. The comparison of mineralogical and geochemical data with previous reconstructions of the Indian monsoon dynamic indicates a rapid response of erosion and sediment transfer of the G-B river system to changes of monsoon rainfall intensity.

1. Introduction

The Bengal deep-sea Fan is the largest submarine fan in the world with a surface of roughly 3.9×10^6 km^2 (3000 km N-S and 1400 km E-W) [*Curray et al.*, 2003]. It is mainly fed in the north by the Ganges-Brahmaputra (G-B) river system [*Curray and Moore*, 1971; *Curray et al.*, 2003] that drains the Himalayas at one of the world's highest physical and chemical erosion rate [*Sarin et al.*, 1989; *Milliman and Meade*, 1983; *Milliman and Syvitski*, 1992]. At present times, most of the sediments from the G-B river system are transferred to the Bengal Fan by a unique submarine canyon, the so-called "Swatch of No Ground" ("SoNG") [*Emmel and Curray*, 1984] (Figure 1). Detrital delivery to the deep-sea fan results from the balance between sediment production (erosion/alteration) in the source areas and their transfer/storage by the fluvial system. As 95% of the sediments originated from the G-B river (about 1×10^9 t yr^{-1}) [*Milliman and Syvitski*, 1992] are transferred to the Bengal Fan during the summer monsoon rainfall, clastic sediments from the Bengal Fan record past changes in the weathering pattern and the transfer of detrital particles, and provide, therefore a record of past regional climatic forcing [*Bouquillon et al.*, 1990; *France-Lanord et al.*, 1993; *Derry and France-Lanord*, 1996; *France-Lanord and Derry*, 1997; *Colin et al.*, 1999; *Joussain et al.*, 2016].

The Indian monsoon results from a differential land-sea sensitive heating between the northern Indian Ocean and the Asian continent (Tibetan Plateau) in response to insolation forcing and is characterized by a seasonal switch in wind direction, precipitation, and runoff [*Webster*, 1987]. The seasonal change in the

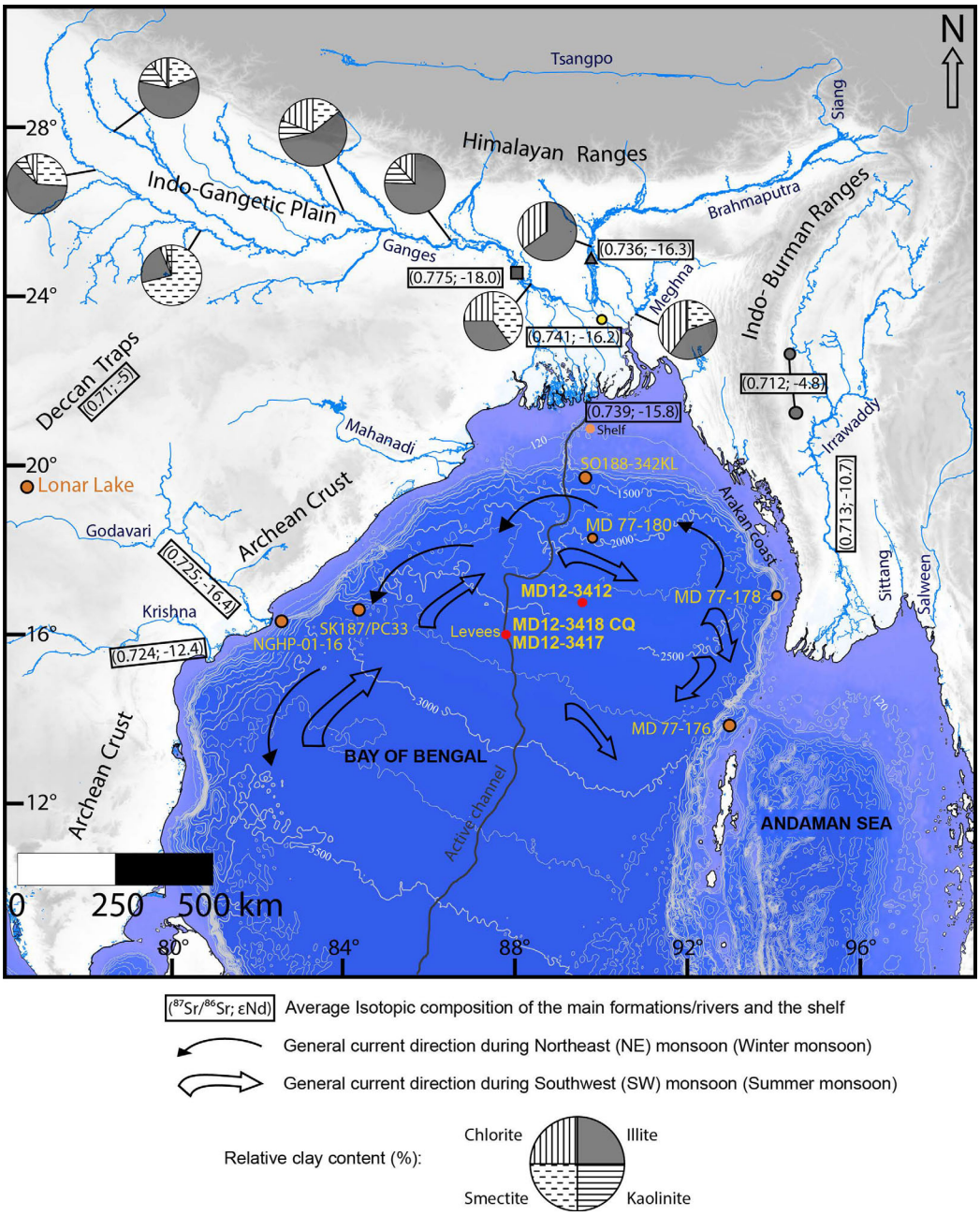

Figure 1. Geographical setting and prevalent hydrography (modified from *Chauhan and Vogelsang* [2006]) of the Bay of Bengal and the surrounding area. Locations of cores discussed in this manuscript are represented by the red dots. Locations of river samples (Ganges, Brahmaputra, and lower Meghna) [*Lupker et al.*, 2013], bulk rock samples from central Myanmar (gray dots) [*Licht et al.*, 2013], and other cores used for comparison (orange dots) [*Tripathy et al.*, 2011, 2014; *Marzin et al.*, 2013; *Contreras-Rosales et al.*, 2014; *Sarkar et al.*, 2015] are also reported. Composite sediment records from the shelf, the middle fan channel levees (in orange) [*Lupker et al.*, 2013] and the average isotopic composition of the main formations/rivers and the shelf ($^{87}Sr/^{86}Sr$ and εNd) are also indicated [*Colin et al.*, 1999, 2006; *Singh et al.*, 2008; *Ahmad et al.*, 2009; *Licht et al.*, 2013; *Lupker et al.*, 2013]. Chart pies represent the clay assemblage of different rivers surrounding the Bay of Bengal [*Huyghe et al.*, 2011, and references therein].

wind direction generates a reversal of surface currents in the Bay of Bengal, which shift from a cyclonic gyre during the winter monsoon to an anticyclonic gyre during the summer monsoon [e.g., *Unger et al.*, 2003; *Chauhan and Vogelsang*, 2006] (Figure 1). Numerous studies have provided insights into the evolution of the Indian summer monsoon intensity over the Indian subcontinent, the Tibetan plateau, and the Himalayas through the Holocene [e.g., *Gasse et al.*, 1991; *Kudrass et al.*, 2001; *Dykoski et al.*, 2005; *Berkelhammer et al.*, 2012; *Cai et al.*, 2012; *Marzin et al.*, 2013; *Contreras-Rosales et al.*, 2014; *Sarkar et al.*, 2015; *Zorzi et al.*, 2015]. It

is now well demonstrated that large-scale Indian monsoon rainfall changes are mainly forced by low-latitude summer solar radiation, which was responsible for changes of thermal contrasted between land and sea [e.g., *Prell*, 1984; *Prell and Kutzbach*, 1987; *Clemens and Prell*, 1991, 2003]. Although orbitally driven summer insolation variations took place gradually, several paleoclimatic records have provided evidence of abrupt changes of the Indian summer monsoon rainfall [*Contreras-Rosales et al*., 2014; *Sarkar et al*., 2015; *Zorzi et al*., 2015] such as relatively more arid conditions and significant discrepancies in the timing and structure of the Holocene humid period around the Bay of Bengal [*Contreras-Rosales et al*., 2014; *Sarkar et al*., 2015; *Zorzi et al*., 2015]. However, recent summer Indian monsoon rainfall record obtained from marine cores of the Bay of Bengal have permitted to reconstruct past variations of monsoon rainfall on G-B river basin and of the northern Bay of Bengal. These results indicate a humid period at the early Holocene before around 6 cal ka BP followed by a gradual decrease of monsoon rainfall between 6 and 4 cal ka BP, and a relatively more arid period since 4 cal ka BP [e.g., *Marzin et al*., 2013; *Contreras-Rosales et al*., 2014]. Such changes in the strength of the Indian summer monsoon had significant impacts on vegetation cover and runoff and could potentially modified weathering of the Himalayas and sediment transport to the Bengal deep-sea Fan. Indeed, several studies conducted on late Quaternary records indicated that the Indian monsoon dynamic could have modulated the sediment budget delivered to the Bay of Bengal [e.g., *Sarkar et al*., 1990; *Colin et al*., 1999, 2006; *Lupker et al*., 2013]. However, climate changes remain difficult to detect from sediments of the Bay of Bengal because their effects can be overprinted by concomitant sea-level changes, which have a strong effect on sedimentation through emergence/flooding of continental shelves and G-B delta that directly affect the morphology of sediment-routing systems, and their ability to deliver sediments to the sea [*Goodbred et al*., 2014; *Joussain et al*., 2016; *Fournier et al*., 2016].

Despite numerous investigations carried out on sea-level changes, morphological evolution of the G-B delta, and climate conditions during the Holocene, results are sometimes controversial and a coherent pattern is still lacking. In the last decades, numerous studies highlight up to three phases of high-amplitude (60 m) sea-level fluctuations in the Bangladesh area [*Umitsu*, 1993; *Goodbred and Kuehl*, 2000; *Islam and Tooley*, 1999; *Rashid et al*., 2013] while *Grant et al*. [2012] depict a significant increase in global the sea-level during the early Holocene (from −40 to −15 m, between 11.5 and 9.2 cal ka BP) followed by a period characterized by a relatively moderate sea-level rise (from −15 to −10 m, between 9.2 and 6.8 cal ka BP) and finally a rather constant sea-level during the middle and late Holocene. In all scenarios, sea-level variations could have modified sedimentary sources and sediment transfer to the Bengal Fan. On the other hand, according to *Weber et al*. [1997], it seems that the present active channel was initiated during the deglaciation, at around 14.5 cal ka BP, in association with an intensification of the summer monsoon, indicating a strong impact of climate changes on sediment transfer to the Bengal Fan. Therefore, effect of sea level on sediments transfer to the northern Bengal deep-sea Fan need to be explored in details prior to any reconstruction of the weathering history of the G-B river system from cores collected on the deep-sea fan.

However, significant changes in weathering patterns of the Himalayas are reflected in the sediment records retrieved on the levee of the active channel of the northern Bengal Fan since the last glacial maximum (LGM) [*Lupker et al*., 2013]. Those sediment deposits suggest an increased chemical weathering during the last deglaciation resulting from an intensification of summer monsoon rainfalls. During the Holocene, variations in chemical weathering state of river sediment discharge are well expressed in the Mekong River basin, where periods of strong monsoon rainfall have been associated with enhanced erosion of the Mekong River lowland favored by the development of incised-valley systems that induced higher inputs of detrital material from the lower reach relative to the upper one of the Mekong River [*Liu et al*., 2004, 2005; *Colin et al*., 2010]. Although such rapid responses of erosion to climatic changes have been observed for several Asian rivers, the G-B river system has not been investigated at a high temporal resolution for the Holocene yet, while this time interval is characterized by an important modification of the monsoon rainfall intensity [e.g., *Fontugne and Duplessy*, 1986; *Weber et al*., 1997; *Kudrass et al*., 2001; *Marzin et al*., 2013; *Contreras-Rosales et al*., 2014].

Up to now, sediments transported by the G-B river system have been intensively studied [e.g., *Galy et al*., 1999; *Galy and France-Lanord*, 1999; *Singh et al*., 2007, 2008; *Garzanti et al*., 2011a, 2011b; *Lupker et al*., 2012]. This is not the case of sediments deposited on the active part of the Bengal Fan that remain poorly documented [*Weber et al*., 1997; *Lupker et al*., 2013; *Fournier et al*., 2016]. However, recent studies have demonstrated that such archives have a great potential to reconstruct the high-resolution history of sediment

dynamic from the G-B river system and assess the effect of summer monsoon changes in the past [*Lupker et al*., 2013; *Fournier et al*., 2016].

In the present study, we conducted for the first time high-resolution (<100 years) clay mineral, Sr, Nd, and major element concentrations analyses, combined with Sr and Nd isotopic measurements on Holocene sediments located in the levee of the active channel, in order to reconstruct (i) the temporal variability of sediment sources and transfer to the Bengal Fan and (ii) changes of the degree of weathering of the sediments from the Himalayan ranges and their potential links to climatic changes. Clay mineral assemblage together with Sr and Nd isotopic compositions of deep-sea sediments from the Bay of Bengal are particularly suitable to establish the main sedimentary sources feeding the Bengal Fan [*Bouquillon et al*., 1989, 1990; *France-Lanord et al*., 1993; *Fagel et al*., 1994, 1997; *Colin et al*., 1999, 2006; *Galy and France-Lanord*, 2001; *Joussain et al*., 2016]. The degree of past chemical weathering of detrital material can also be estimated from the study of major elements concentrations and more especially of the immobile (Si, Al, and Fe) versus mobile (K) elements after to have taken into account size-sorting process of minerals during transport [*Lupker et al*., 2013].

2. Material and Methods

2.1. Studied Cores and Chronological Framework

Long Calypso Core MD12–3417 (16°30.03′N, 87°47.82′E; water depth 2556 m, length 39.8 m) and the relatively short CASQ Core MD12–3418CQ (16°30.27′N, 87°47.92′E; water depth 2557 m, length 8.5 m) were both retrieved on the eastern levee of the active channel during the MD191/MONOPOL expedition of the French R/V *Marion Dufresne*, in May–June 2012 (Figure 1). The sediments of both cores are chiefly characterized by a dark olive mud interlayered with silty and sandy laminations corresponding to turbidite deposits [*Fournier et al*., 2016].

A composite sediment record has been obtained thanks to the correlation of very high resolution (1 cm spacing) XRF geochemical data, measured on both cores with an Avaatech XRF core-scanner, as described by *Fournier et al*. [2016]. This method described in detail in *Fournier et al*. [2016] also allowed an identification of the turbidites layers. The age models of cores MD12–3418CQ and MD12–3417 were based on 13 AMS ^{14}C measurements (five on Core MD12–3418CQ and eight on Core MD12–3417) performed on shallow-dwelling planktonic foraminifera (*Globigerinoides ruber*, *Globigerinoides trilobus*, and *Globigerinoides sacculifer*). Radiocarbon ages were converted into calendar ages using the Marine-13 calibration curve [*Reimer et al*., 2013] and Calib 7.0.2. The calibration integrates an average ocean reservoir effect of 400 years [*Stuiver and Reimer*, 1993], which is close to the reservoir age estimated in this area [*Southon et al*., 2002]. The composite core represents a continuous sedimentary record of the last 9.8 cal ka BP (Figure 2). Sedimentation rates vary from <0.1 to 5 cm yr^{-1}. The extremely high sedimentation rate (around 5 cm yr^{-1}) observed from 33.9 to 10.4 m (i.e., from 9.8 to 9.2 cal ka BP) in the composite sediment record is attributed to intense turbidite activity [*Fournier et al*., 2016]. After 9.2 kyr (i.e., 10.4 m), even if turbiditic activity is sporadically detected from 9.2 to 5.6 cal ka BP and after 2.6 cal ka BP [*Fournier et al*., 2016], sedimentation rates dropped drastically to an average of 0.1 cm yr^{-1}.

In order to insure the construction of continuous composite mineralogical and geochemical records, samples were collected with an overlap of 23 cm (i.e., 200 years) between the two cores. A total of 400 samples were studied for clay mineralogy determinations. From these 400 samples, 124 and 24 have been selected for major element concentrations and Sr and Nd isotopic compositions analyses, respectively. Sampling strategy was adapted to the age model, with a reduction of the sampling spacing in the (upper) interval characterized by lower sedimentation rates. For clay mineralogy analyses the time resolution is lower than 50 years from 9.8 to 9.2 cal ka BP and around 100 years after 9.2 cal ka BP.

2.2. Clay Mineralogical Analyses

X-ray diffraction (XRD) identification of clay minerals was conducted on oriented mounts of the carbonate-free <2 μm fraction, using a PANalytical X'Pert Pro Diffractometer at the State Key Laboratory of Marine Geology, Tongji University. Bulk sediments were first leached using 0.1 N HCl in order to remove carbonates. The mixtures were then rinsed several times to remove the acid residues. The <2 μm fraction was subsequently separated by settling according to the Stoke's law. XRD analyses were performed using CuKα

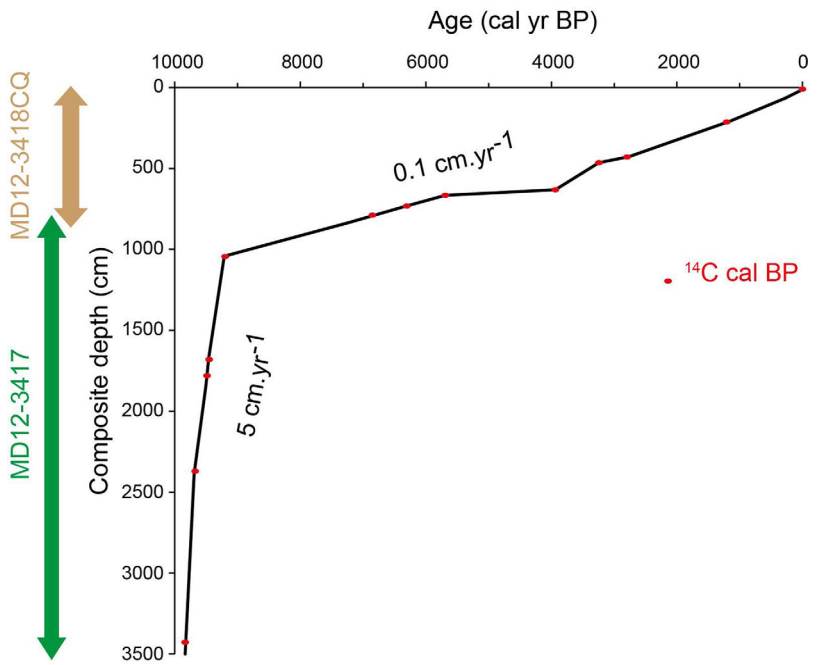

Figure 2. The time scale of the composite record of Cores MD12–3418CQ and MD12–3417 is obtained by combining ^{14}C AMS ages and correlating XRF records from both cores [*Fournier et al.*, 2016]. The lower part of the record is characterized by very high sedimentation rates (around 5 cm yr^{-1}) due to an intense turbiditic activity associated to enormous sedimentary fluxes, associated with the formation of the levee of the actual channel. After 9.2 cal ka BP, sedimentation rates dropped drastically (around 0.1 cm yr^{-1}). The light brown and green arrows represents the intervals of Cores MD12–3418CQ and MD12–3417 spliced in the composite record, respectively.

radiation and Ni filter, under 40 kV and an intensity of 25 mA under three different conditions: air-dried, ethylene glycol-saturated, and heated (490°C for 2 h) [*Holtzapffel*, 1985]. The samples were X-rayed in the range 3–30° 2Θ with a step increment of 0.03° 2Θ and a measurement time of 1 s/step. Semiquantitative estimates of peak areas of the basal reflections of smectite (15–17 Å), illite (10 Å), and kaolinite/chlorite (7 Å) were carried out on the glycolated curve using MacDiff software [*Petschick*, 2000]. Relative proportions of kaolinite and chlorite were estimated from the ratios of areas of the (002) peak of kaolinite (3.57 Å) and the (004) peak of chlorite (3.54 Å). The semiquantitative evaluation of each clay mineral has an accuracy of ∼5%.

2.3. Geochemical Analyses

Major elements, Sr and Nd concentrations, and Sr-Nd isotopic compositions were performed on carbonate-free samples. Carbonates were removed by leaching processes with a 20% acetic acid solution in an ultrasonic bath. Samples were rinsed and centrifuged five times.

For major elements and Sr and Nd concentrations, about 30–40 mg of carbonate-free sediments were heated at 600°C to obtain the loss of ignition (LOI). The samples were then dissolved using a mixed solution of HNO_3-HF on a hot plate, and diluted with 2% HNO_3. Measurements have been performed at the State Key Laboratory of Marine Geology (Tongji University), using an Iris Advantage ICP-OES. Such analytical procedure does not permit direct Si measurement. The SiO_2 concentrations were obtained as the complement to 100% after subtracting all other major-element concentrations and LOI. Replicate analyses of reference samples (GSR-5, GSR-6, and GSD-9) gave an accuracy of 10% for Si and of 4% for all other major elements. Replicate analyses of samples gave a precision of ±3% (2σ). Sr and Nd concentrations were analyzed by inductively coupled plasma-mass spectrometry (ICP-MS) using a Thermo VG-X7 mass spectrometer at the State Key Laboratory of Marine Geology, Tongji University. Uncertainties for Sr and Nd concentrations are <3% (2σ).

Nd and Sr isotopic compositions were analyzed using a Thermo Scientific Multi-Collector Induced Coupled Plasma Mass Spectrometer (MC-ICPMS NEPTUNE^{Plus}) at the Laboratoire des Sciences du Climat et de l'Environnement (LSCE) in Gif-sur-Yvette. Carbonate-free samples were first dissolved in HF-$HClO_4$ and HNO_3-HCl

mixtures. An initial chemical separation has been operated using Biorad columns packed with AG50WX-8, and 200–400 mesh cationic exchange resin. Sr and REE elements were isolated using 2 N HCl and 2.5 N HNO_3 solutions, respectively. The Sr fraction was purified on a 20 µl SrSpec column consisting of a polyethylene syringe with a 4 mm Ø millex filter. Nd was extracted and purified from REEs fraction using an Ln-Spec column following the method described in details by *Copard et al.* [2010]. In this method, samples were loaded using 0.7 mL of 0.05 N HNO_3 on preconditioned LN-Spec columns. The Sr and Nd isotopic compositions were analyzed at a concentration of 15 ppb. During the analytical sessions, every two samples were bracketed with analyses of appropriate Sr standard solution NIST SRM987 characterized by certified values of 0.710250. For the analyses of the Nd isotopic composition, samples were bracketed using Nd standard solutions JNdi-1 and La Jolla characterized by certified values of 0.512115 ± 0.000006 [*Tanaka et al.*, 2000] and 0.511858 ± 0.000007 [*Lugmair et al.*, 1983], respectively. Standard solutions were analyzed at concentrations similar to those of the samples and we have corrected all of the measurements affected by analytical bias when necessary. The mass-fractionation correction was made by normalizing $^{146}Nd/^{144}Nd$ to 0.7219 and $^{86}Sr/^{88}Sr$ to 0.1194 and applying an exponential-fractionation correction.

3. Results

3.1. Clay Mineralogy

The clay mineral assemblage of the composite core consists mainly of smectite (24–57%), illite (24–48%), and chlorite (15–24%). Kaolinite proportions are low and display only slight variations (3–8%) that will not be discussed further (Figure 3). In general, illite and chlorite contents display relatively similar distributions and are inversely correlated to smectite contents. During the early Holocene (between 9.8 and 6 cal ka BP) clay fraction is characterized by lower proportions of smectite (from 24 to 43%) and higher contents of illite (from 33 to 48%) and chlorite (from 17 to 24%) than the late Holocene. In detail, this time interval is characterized by lowest smectite proportions between 9.2 and 7 cal ka BP (from 26 to 38%) and around 5.9 cal ka BP (31%). Between 5.5 and 4.0 cal ka BP, smectite content display significantly higher values (from 35 to

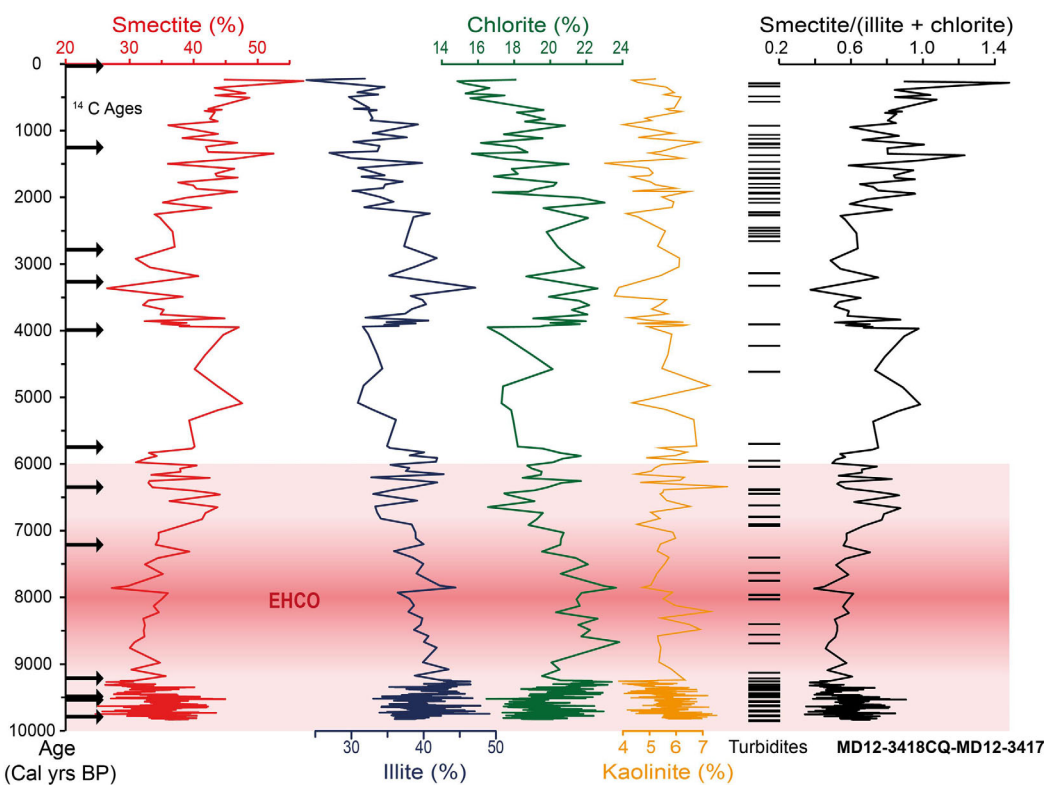

Figure 3. Clay mineral proportions (%) in the <2 µm size fraction, and smectite/(illite+chlorite) ratio (cal ka BP) for the composite record. ^{14}C AMS ages, turbidite layers identified by *Fournier et al.* [2016], and the Early Holocene Climatic Optimum (EHCO) are also displayed.

50%), before rapidly decreasing up to 26% at 3.4 cal ka BP. This increase in smectite contents (between 5.5 and 4.0 cal ka BP) is associated with a decrease in illite and chlorite contents, from 41 to 31% and 22 to 16%, respectively. After 3.4 cal ka BP, the proportions of smectite increase from 26 to 57% while illite and chlorite contents decrease from 47 to 24% and 20 to 15%, respectively.

As smectite variations tend to be opposed to those of illite and chlorite, we reported the smectite/(illite+-chlorite) ratios in Figure 3 in order to highlight the main mineralogical changes recorded within the clay fraction. This mineralogical ratio ranges from 0.34 to 1.48. It is generally characterized by low values (0.34–0.91) in the early Holocene (from 9.8 to 5.9 cal ka BP) with the lowest values between 9.2 and 7 cal ka BP (from 0.37 to 0.7). Then it increases from 5.9 to 5 cal ka BP to reach a value of 0.99, and decrease up to 0.38 at 3.4 cal ka BP. The late Holocene (after 3.4 cal ka BP) is associated with an increase of the smectite/(illite+chlorite) ratio to a value of 1.48 with significantly lower values (around 0.6 to 0.8) around 1 cal ka BP.

3.2. Major Elements

Carbonate-free sediments of the composite core consist mainly of Si, Al, Fe, Mg, and K, with low concentrations of Na, Ca, Ti, and Mn. Fe, Al, and Si are considered to be immobile elements during the Himalayan erosion and are therefore not significantly affected by chemical weathering [*Galy and France-Lanord*, 2001; *Lupker et al*., 2012]. They are associated with the persistent, initial chemical signature of the weathered rocks. Potassium, on the other hand, is a mobile element and can be used to trace the degree of chemical weathering experienced by sediments of the G-B river and the northern Bay of Bengal [*Lupker et al*., 2012, 2013]. In general, Si contents are inversely correlated to Al ($r^2 = 0.82$) and Fe ($r^2 = 0.72$). Al/Si and Fe/Si are reported in Figure 4b together with K/Al.

Sediments of the time interval from 9.8 and 9.2 cal ka BP are characterized by low Al/Si and Fe/Si ratios, ranging from 0.22 to 0.41 and from 0.06 to 0.1, respectively. After 9.2 cal ka BP, sediments are characterized by relatively high Al/Si and Fe/Si ratios, fluctuating from 0.3 to 0.43 and 0.08 to 0.13, respectively (Figure 4b). The correlation obtained between Al/Si and Fe/Si ratios (Figure 4a) represents mainly the mineralogical segregations that occur during sediment transport to the Bengal Fan [*Lupker et al*., 2011, 2013]. The K/Al ratio is characterized by relatively high values between 9.8 and 9.2 cal ka BP and between 7 and 5.3 cal ka BP, ranging from 0.21 to 0.25 and from 0.20 to 0.21, respectively. On the contrary, time interval from 9.2 to 7 cal ka BP and from 5.3 to 4 cal ka BP are associated to lower values ranges from 0.19 to 0.21. After 4 cal ka BP, the K/Al ratio decrease slightly to reach a value of 0.19 at present time.

3.3. Sr and Nd Concentrations and Isotopic Compositions

Sr and Nd concentrations, $^{87}Sr/^{86}Sr$ ratios, and εNd values obtained on the composite core are reported in Table 1. Sr and Nd concentrations range from 75.2 to 111.9 ppm and from 31.8 to 43.3 ppm, which is in agreement with values previously obtained for sediments of the Bay of Bengal [*Bouquillon et al*., 1990; *Colin et al*., 1999, 2006; *France-Lanord et al*., 1993; *Galy and France-Lanord*, 2001; *Goldstein and Jacobsen*, 1988; *Pierson-Wickmann et al*., 2001; *Lupker et al*., 2013]. εNd values range from −16.6 to −12.6 (mean value of −15.1). $^{87}Sr/^{86}Sr$ ratio varies from 0.744 to 0.753 (mean value of 0.749) (Table 1 and Figure 5). Changes of the smectite/(illite+chlorite) ratio are not associated to any systematic variations of the $^{87}Sr/^{86}Sr$ ratios and εNd values (Figure 5), as there is no increasing or decreasing trend of the Sr and Nd isotopic compositions through the Holocene.

4. Discussion

4.1. Levee Construction and Turbiditic Activity

In the composite record, clay mineralogical determinations were conducted on both, the fine-grained hemipelagic layers and the turbidite layers as identified by *Fournier et al*. [2016]. In the northern Bay of Bengal, the size range of smectite (between 0.1 and 1 μm) is lower than those of illite and chlorite (between 0.5 and 4 μm) [*Bouquillon et al*., 1989, 1990; *France-Lanord et al*., 1993]. Thus, transport of sediments associated to turbidite activity could potentially modify the clay assemblage through sorting mechanisms and differences in the size and/or floating properties of clay minerals [*Liu and Li*, 2011]. Such processes have been already described on the continental shelves off river mouths [*Gibbs*, 1977; *Patchineelam and De Figueiredo*, 2000; *Liu et al*., 2010] and at lesser extend discussed for deep-sea environments [*Liu and Li*, 2011; *Liu et al*., 2016; *Joussain et al*., 2016].

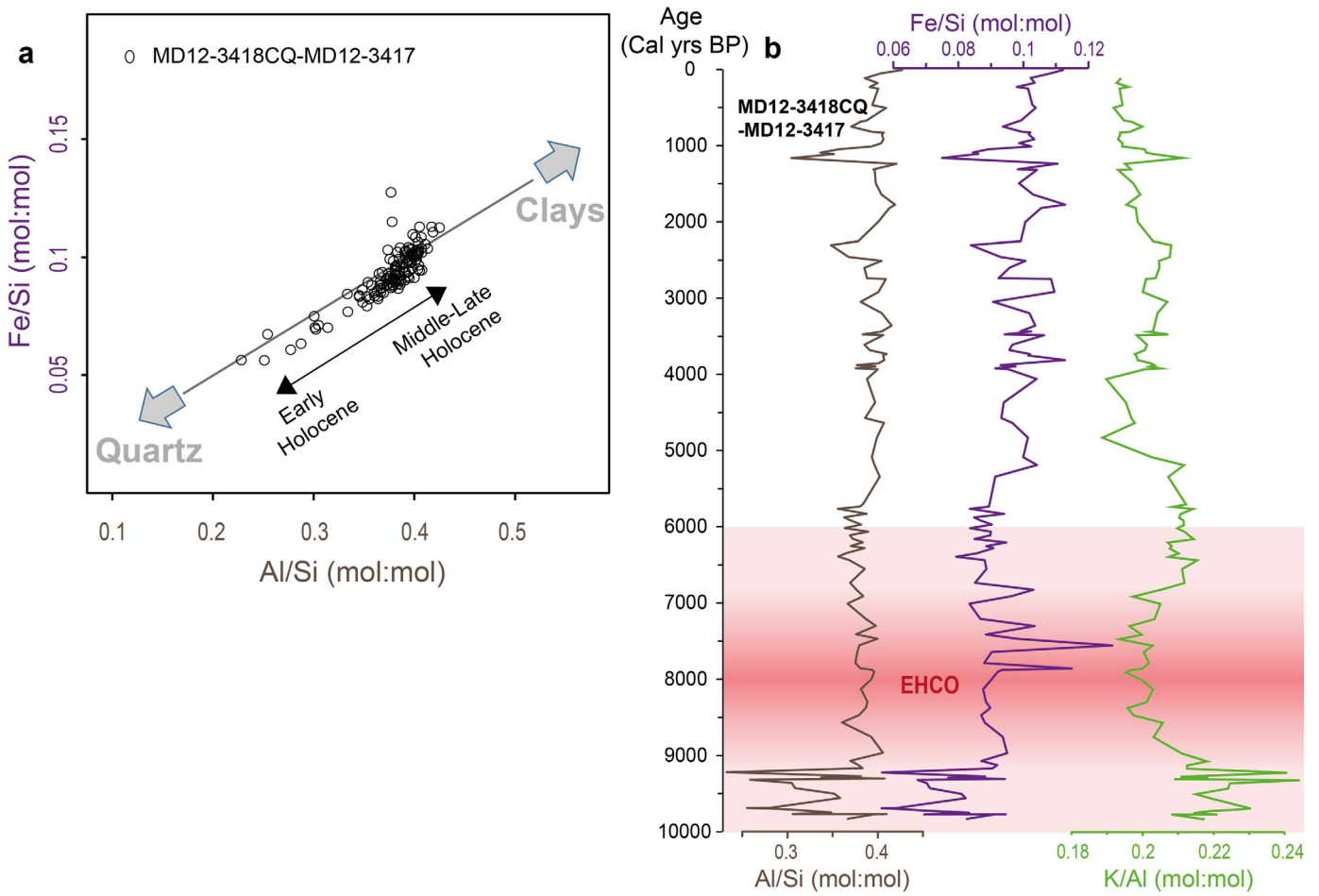

Figure 4. (a) Diagram of Fe/Si versus Al/Si ratios displaying hydraulic sorting effect on the Si-Al-Fe chemical compositions of sediments. Sediments from our composite records are the result of the mixing between a low Al/Si and Fe/Si quartz-rich coarse-grained end-member and a high Al/Si and Fe/Si surface end-member relatively enriched in phyllosilicates (gray line). (b) variations of Al/Si, Fe/Si, and K/Al ratios of the composite core. Early Holocene Climatic Optimum (EHCO) is also displayed.

As far as turbiditic activity is concerned, two major phases have been identified during the levee construction: (i) the first phase (i.e., initial construction of the levee) took place before 9.2 cal ka BP and is characterized by a very intense turbiditic activity, which resulted in extremely high sedimentation rates (5 cm yr^{-1}) [*Fournier et al.*, 2016]; (ii) the second phase took place from 9.2 cal ka BP to the present time and is characterized by sporadic turbiditic activity resulting in lower sedimentation rates ($<$0.1 cm yr^{-1}). Interestingly, the turbidite layers do not show the highest proportions of illite and chlorite. Inversely, hemipelagic layers are not systematically enriched in smectite (Figure 3 and Table 1). More precisely, periods of increased turbidite activity are not systematically associated with decreased smectite/(illite+chlorite) ratio in the studied samples. All these findings suggest that sedimentary processes, and particularly turbidite activity associated to the construction of the levee as well as the mode and strength of the gravity currents, are not responsible for significant changes in the clay mineral assemblage. Such results are in agreement with clay mineralogical analyses already performed on turbidite and hemipelagic layers of Core MD12–3412 located in the northeastern part of the fan, which is not actually under the direct influence of the active channel [*Joussain et al.*, 2016].

One of the most plausible factors that could produce such drastic changes in sediments are rapid variations in the sea level. The abrupt sea-level rise that occurred at 9.2 ka BP is accompanied by an increase in the accommodation space available on the inner continental shelf [*Fournier et al.*, 2016] that could increase the efficiency of sediment storage on the continental shelf and ultimately, result in important reduction in the turbidite activity on the active middle fan channel levee [*Weber et al.*, 1997; *Fournier et al.*, 2016]. *Fournier et al.* [2016] suggested that the low sea-level and the strengthening of the Indian monsoon recorded

Table 1. Sample Depths (cm) in Core, Type of Deposits (T: Turbidite Layers, HP: Hemipelagic Layers), Age of the Sediments (Cal ka BP), Sr and Nd Concentrations (ppm), $^{87}Sr/^{86}Sr$, $^{143}Nd/^{144}Nd$, and εNd Values As Well As Smectite (Smec), Illite (Ill), Chlorite (Chl), and Kaolinite (Kaol) Proportions (%) for All Studied Core Samples Investigated in This Study[a]

Sample Depth[b] (cm)	Age (yr Cal BP)	HP-T	Sr (ppm)	$^{87}Sr/^{86}Sr$	±2σ	Nd (ppm)	$^{143}Nd/^{144}Nd$	±2σ	εNd (0)	±2σ	Smec (%)	Ill (%)	Chl (%)	Kaol (%)
Core MD12–3418CQ; Location 16°30′27″ N, 87°47′92″ E; Water Depth = 2557 m														
0	Modern	HP	97.1	0.74754	0.00002	42.0	0.511915	0.000014	−13.8	0.26	n.a	n.a	n.a	n.a
165	912.15	T	93.6	0.74730	0.00002	39.6	0.511855	0.000014	−15.0	0.26	36	39	21	4
202	1156.45	T	108.2	0.74797	0.00002	37.6	0.511832	0.000014	−15.4	0.26	n.a	n.a	n.a	n.a
319	1996.94	HP	107.4	0.74383	0.00002	41.5	0.511869	0.000014	−14.6	0.26	39	34	22	5
375	2453.45	T	98.1	0.75026	0.00002	42.0	0.511869	0.000014	−14.7	0.26	n.a	n.a	n.a	n.a
388	2504.13	T	97.7	0.74957	0.00002	43.3	0.511836	0.000014	−15.3	0.26	37	38	20	6
445	3041.97	T	103.6	0.74851	0.00002	42.2	0.511838	0.000014	−15.2	0.26	33	39	22	6
486	3353.7	HP	93.2	0.74860	0.00002	37.8	0.511848	0.000014	−15.1	0.26	26	47	23	4
594	3804.82	HP	83.5	0.74981	0.00002	36.8	0.511838	0.000014	−15.2	0.26	45	32	19	4
620	3913.42	T	88.8	0.75108	0.00002	36.4	0.511849	0.000014	−14.9	0.26	39	35	20	6
623	3925.95	T	91.2	0.75106	0.00002	37.9	0.511762	0.000014	−16.6	0.26	38	37	19	6
652	5181.76	HP	81.5	0.75236	0.00002	35.1	0.511829	0.000014	−15.5	0.26	44	33	18	6
695	6010.76	HP	88.7	0.75006	0.00002	34.7	0.511975	0.000014	−12.6	0.26	40	35	19	5
735	6385.23	HP	89.2	0.75175	0.00002	37.6	0.511838	0.000014	−13.8	0.26	40	36	19	6
Core MD12–3417; Location 16°30′03″N, 87°47′82″ E; Water Depth = 2564 m														
1236	7780.25	T	95.2	0.74483	0.00002	39.3	0.511860	0.000014	−15.3	0.26	n.a	n.a	n.a	n.a
1334	8746.56	T	105.2	0.74873	0.00002	37.7	0.511845	0.000014	−14.9	0.26	30	42	23	5
1357	8958.52	HP	98.4	0.75302	0.00002	38.3	0.511846	0.000014	−15.1	0.26	35	40	20	5
1368	9063.15	T	98.7	0.75196	0.00002	38.7	0.511826	0.000014	−15.1	0.26	30	43	21	6
2070	9494.42	T	84.8	0.75146	0.00002	37.8	0.511845	0.000014	−15.5	0.26	36	39	20	5
2964	9740.35	HP	88.9	0.74904	0.00002	38.7	0.511829	0.000014	−15.1	0.26	36	39	19	6
3130	9762.16	T	82.3	0.74858	0.00002	38.0	0.511817	0.000014	−15.6	0.26	34	39	20	6
3137	9762.3	T	83.1	0.74737	0.00002	39.4	0.511853	0.000014	−15.9	0.26	37	37	19	7
3141	9763.21	T	86.7	0.74688	0.00002	39.7	0.511833	0.000014	−15.3	0.26	40	36	17	7
3740	9824.45	HP	79.7	0.74969	0.00002	40.0	0.511824	0.000014	−15.7	0.26	n.a	n.a	n.a	n.a

[a]Locations and water depth (m) of all cores have been also reported. εNd was determined using the present CHUR value from *Jacobsen and Wasserburg* [1980], εNd (0) = $[(^{143}Nd/^{144}Nd)_{meas}/0.512638 - 1] * 10000$. 2σ standard deviation derived from the reproducibility of NIST SRM987 or La Jolla standards over each analytical run. If the internal 2σ was larger than the external one, the internal error is reported. n.a.: not analyzed.
[b]Sample depth (cm, not corrected).

before 9.2 ka cal BP favored a strong connection between rivers and the Bengal Fan, as assessed by the high sedimentation rates and the rapid construction of well-developed levees. After 9.2 ka cal BP, the sedimentation rates declined abruptly probably due to the higher sea level leading to a partial disconnection between massive river discharges and the deep turbidite system.

4.2. Sediment and Clay Mineral Sources

In order to constrain the sedimentary sources of the active part of the Bengal Fan and its variations through the Holocene, the εNd values and $^{87}Sr/^{86}Sr$ ratio obtained herein are presented within a cross plot (Figure 6) together with data obtained on sediments from the northern Bay of Bengal (Bengal shelf, northern Bay of Bengal in and outside of the levee system [*Colin et al*., 1999, 2006; *Lupker et al*., 2013; *Joussain et al*., 2016] and the main rivers feeding the Bengal Fan [*Galy and France-Lanord*, 2001; *Singh and France-Lanord*, 2002; *Singh et al*., 2008; *Tripathy et al*., 2011]) (Figure 6). In this diagram, mixtures of sediments from two different sources align along a hyperbolic curve, whose shape depends on the end-member Sr/Nd concentration ratios.

The studied samples are characterized by εNd values from −16.6 to −12.6 and $^{87}Sr/^{86}Sr$ from 0.744 to 0.753 that are in the range of isotopic compositions previously obtained on Holocene sediments from (i) the Bay of Bengal: in the middle fan channel levees (Cores SO93–117KL, 118KL and 120KL with εNd values from −17.3 to −14.5 and $^{87}Sr/^{86}Sr$ ratios from 0.728 to 0.749), and in the proximal shelf (Cores SO93–105KL and 107KL with εNd values from −16.1 to −15.4 and $^{87}Sr/^{86}Sr$ ratios from 0.734 to 0.743) [*Lupker et al*., 2013]; (ii) river sediments: the Lower Meghna (confluent of G-B rivers; εNd from −17.0 to −13.7 and $^{87}Sr/^{86}Sr$ ratios from 0.723 to 0.746) [*Lupker et al*., 2013]. Such values contrast with those obtained on sediments from the northeastern nonactive part of the Bengal Fan [*Colin et al*., 1999; *Joussain et al*., 2016] and exclude sediments deriving from the Indo-Burman ranges which are characterized by εNd values and $^{87}Sr/^{86}Sr$ ratios ranging from −7.8 to +0.3 and from 0.705 to 0.718, respectively [*Licht et al*., 2013] (Figure 6). This implies that sediments from Cores MD12–3417 and MD12–3418CQ located off the active channel of

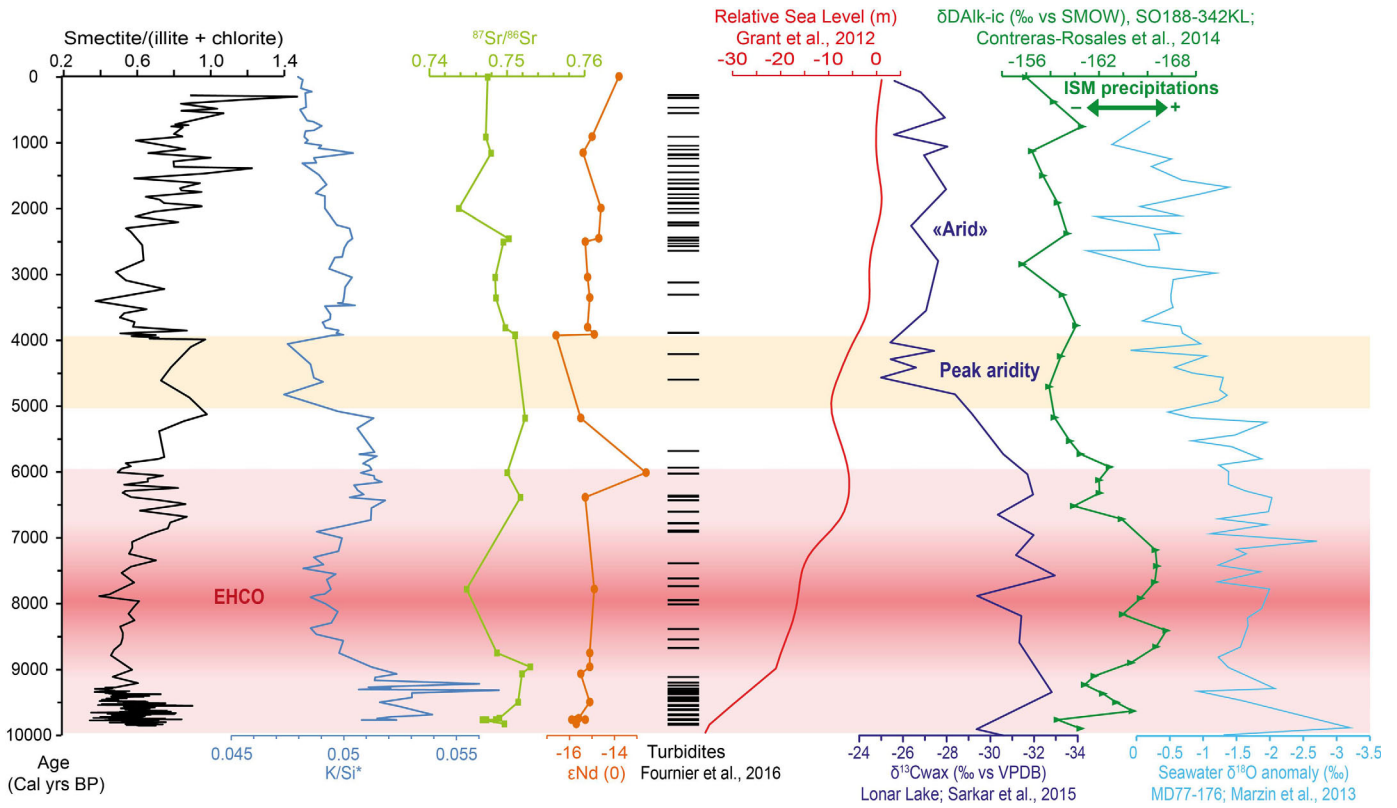

Figure 5. Smectite/(illite + chlorite), K/Si*, εNd, and $^{87}Sr/^{86}Sr$ values of the carbonate free-fraction versus age (cal yr BP) of the composite record. Turbidite layers identified by *Fournier et al*. [2016], relative sea level [*Grant et al*., 2012], Lonar lake $\delta^{13}C$ record [*Sarkar et al*., 2015]; δDAlk-ic record from Core SO188–342KL [*Contreras-Rosales et al*., 2014], seawater $\delta^{18}O$ anomaly [*Marzin et al*., 2013], and the Early Holocene Climatic Optimum (EHCO) are also displayed. The light orange box represents the aridity peak identified by [*Sarkar et al*., 2015]. ISM stands for the Indian Summer Monsoon.

the Bengal Fan, derived mainly from the G-B river system (Figure 6) in agreement with previous results obtained by *Lupker et al*. [2013] on sediments of the active channel levee. Interestingly, εNd values and $^{87}Sr/^{86}Sr$ ratios obtained on the turbidite layers are similar to those measured on the hemipelagic layers, indicating a contribution of the G-B river system to both types of sediments (Table 1 and Figure 6). Furthermore, Nd and Sr isotopic compositions from our composite record match those recorded in the High Himalaya Crystalline rocks (HHC), which range in average between −16 and −14.5 for εNd values and between 0.735 and 0.760 for $^{87}Sr/^{86}Sr$ ratios, Figure 6). Such results confirm previous studies and indicate that the HHC rocks are the main sedimentary source to the Indo-Gangetic plain and the eastern Bengal Fan [*France-Lanord et al*., 1993; *Galy et al*., 1996; *Colin et al*., 1999; *Galy and France-Lanord*, 2001; *Singh and France-Lanord*, 2002; *Tripathy et al*., 2011; *Lupker et al*., 2013].

Although the results of Nd and Sr isotope data indicate a unique source of sediments corresponding to the G-B river system, the smectite/(illite+chlorite) ratio presents large variations during the Holocene, with relatively high values during the 7.0–5.9, 5.5–4.0, and 2.5–0 cal ka BP time intervals. Such pattern reflects a modification in the mineralogical composition of detrital inputs within the G-B river system, and particularly, distinct mineralogical signatures between the Highlands and the Indo-Gangetic floodplain [*France-Lanord et al*., 1993; *Colin et al*., 1999; *Joussain et al*., 2016]. Indeed, as complemented by studies of river-bank material and suspended sediments in the Ganges River [*Sarin et al*., 1989; *Huyghe et al*., 2011] and the Indo-Gangetic floodplain [*Sarin et al*., 1989; *Huyghe et al*., 2011], it appears that illite and chlorite are mainly produced by intensive physical erosion of the metamorphic and granitic rocks that characterize the highlands, while smectite mainly derives from chemical weathering of primary minerals in the Indo-Gangetic floodplain. In such a context, smectite mainly derives from the recycling of the Siwalik Group sedimentary rocks, which are particularly enriched in smectite, and from pedogenic processes within the Ganges River plain [*Huyghe et al*., 2011]. In the Indo-Gangetic plain, clay contents are locally very different, but in average smectite content is estimated between 60 and 20%, illite 50 and 20%, chlorite 15 and 25%, and kaolinite 5 and

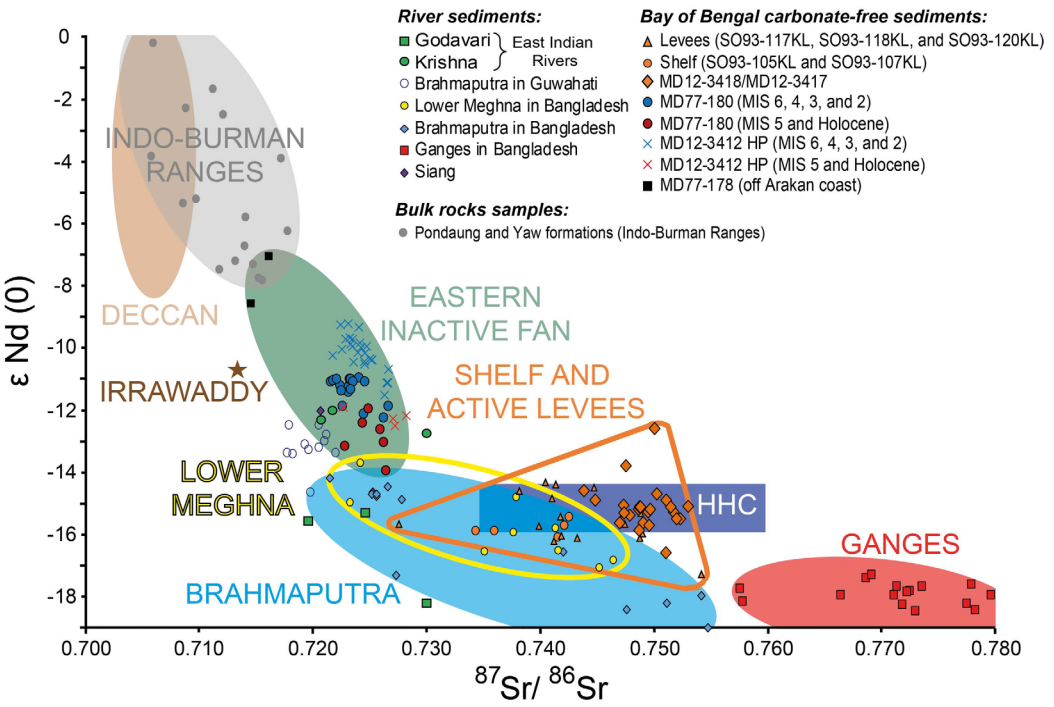

Figure 6. Variations of εNd versus $^{87}Sr/^{86}Sr$ of the composite core (Cores MD12–3418CQ/MD12–3417), Cores MD12–3412 HP (HP: hemipelagic sediments, *Joussain et al.*, 2016) and MD77–180 (detrital fraction) compared to cores, rivers sediments and bulk rock samples around the Bay of Bengal. In this diagram, we grouped data from Indian river samples (Godavari and Krishna) [*Ahmad et al.*, 2009], different parts of the modern G-B river system (samples from the Siang, Brahmaputra, Ganges, and Lower Meghna) [*Singh and France-Lanord*, 2002; *Lupker et al.*, 2013], the shelf and the levees of the northern part of the Bay of Bengal [*Lupker et al.*, 2013]. Sediments from cores MD77–178 (off the Arakan coast), MD77–176 (off the mouth of the Irrawaddy River), a sample from the Irrawaddy River [*Colin et al.*, 1999, 2006], formations from the Indo-Burman ranges (Pondaung and Yaw formations) [*Licht et al.*, 2013], and from the Deccan Traps [*Peng et al.*, 1994; *Singh et al.*, 2008] are also plotted. The isotopic composition of the High Himalaya Crystalline (HHC) are from *Galy et al.* [1996] and *Galy and France-Lanord* [2001, and references therein].

10% [*Sarin et al.*, 1989; *Huyghe et al.*, 2011]. Smectite could partly originate from the weathering of the basaltic Deccan Traps as observed in the western Bay of Bengal (Core SK187/PC33 in Figure 1) [*Tripathy et al.*, 2011, 2014]. However, such contribution can be ruled out in our record since Deccan Traps is characterized by Nd and Sr isotopic compositions (εNd values from −13 to +5 with a mean εNd ≈ −5; $^{87}Sr/^{86}Sr$ from 0.704 to 0.716 with a mean $^{87}Sr/^{86}Sr \approx 0.710$ [*Singh et al.*, 2008], Figure 6) that are clearly distinct from the isotopic signature of sediments retrieved in the G-B river system (εNd values from −18.5 to −13.5 and $^{87}Sr/^{86}Sr$ ratios from 0.720 to 0.790; Figure 6). Such results confirm geochemical (major element, Sr, and Nd isotopic compositions) and mineralogical (spatial distribution of clay assemblages) studies conducted on the eastern inactive part of the Bengal Fan that have previously shown that smectite from the Deccan Traps does not feed the northern Bay of Bengal [*Bouquillon et al.*, 1989; *Colin et al.*, 1999; *Joussain et al.*, 2016].

4.3. Ganges-Brahmaputra-Meghna Delta Migration and Dynamics of Sediment Transport

The clay mineralogical composition of sediments from the Brahmaputra River is not well constrained. However, it appears for its downstream section to be dominated by illite (60–70%) and chlorite (30–40%), while smectite is absent (Figure 1). On the other hand, the downstream of the Ganges River is characterized by relative high smectite (20–60%) and lower illite (20–50%), and chlorite (20–30%) contents. Such pattern implies an important contrast in the clay mineralogical compositions of sediments between the Ganges and the Brahmaputra rivers [*Sarin et al.*, 1989; *Huyghe et al.*, 2011] (Figure 1). Therefore, variations of smectite/(illite+chlorite) ratio through the Holocene could also reflect changes in the relative contribution of sediments deriving from the Ganges and Brahmaputra rivers. Such changes could be induced either by variations in the morphology of the G-B delta (modification of the fluvial channel positions on the delta, as described by *Goodbred et al.* [2014]), or by variations in the relative sediment discharge of these rivers. According to *Goodbred et al.* [2014], during the early and middle Holocene, the fluvial channel positions of the downstream Ganges and Brahmaputra rivers were constrained to their respective lowstand valleys. It is

only at around 6 cal ka BP that the Ganges channel system began to shift eastward, while the Brahmaputra system was occupying the Sylhet basin (located to the east of the modern position). Such migration pattern is confirmed at around 3 cal ka BP, when sediments from the Ganges River became dominant in the central part of the delta [*Goodbred et al*., 2014; *Pickering et al*., 2014]. It could have affected sediment distribution and storage in and around the G-B delta.

Sediments from the Ganges and Brahmaputra rivers are characterized by contrasted εNd values and $^{87}Sr/^{86}Sr$ ratios. εNd and $^{87}Sr/^{86}Sr$ range from −18.5 to −16.5 and from 0.755 to 0.790 in the Ganges, while εNd and $^{87}Sr/^{86}Sr$ fluctuate between −18.5 and −13.5 and between 0.720 and 0.735 in the Brahmaputra, respectively (Figure 6) [*Sarin et al*., 1989; *Huyghe et al*., 2011; *Singh and France-Lanord*, 2002; *Singh et al*., 2008; *Lupker et al*., 2013; *Goodbred et al*., 2014]. Sediments from the Lower Meghna, corresponding to the confluence of the Ganges and the Brahmaputra, are characterized by εNd and $^{87}Sr/^{86}Sr$ values fluctuating from −17.0 to −13.7 and from 0.724 to 0.746, respectively [*Lupker et al*., 2013]. Sr and Nd isotopic compositions obtained from sediments of the middle fan channel levees remain quite constant, being in the range of the modern G-B river sediment samples [*Lupker et al*., 2013]. Besides, changes in the smectite/(illite+-chlorite) ratio from 7 to 4 cal ka BP are recorded during time intervals characterized by relative morphological stability in the Ganges-Brahmaputra-Meghna delta [*Goodbred et al*., 2014]. It is only during the late Holocene (the last 2.5 cal ka BP) that the increase of the smectite/(illite+chlorite) ratio could be associated to a stronger discharge of the Ganges River as it has shifted to the center of the delta. However, such pattern is ruled out by the narrow ranges of εNd and $^{87}Sr/^{86}Sr$ values obtained on the sediments from the active levee (–15.3 to −13.8 for εNd and 0.744 to 0.750 for $^{87}Sr/^{86}Sr$) that do not display a higher contribution of the Ganges River during that time interval. All these results suggest that the relative contribution of Ganges and Brahmaputra rivers to the Bengal Fan, potentially induced by a modification of the position of the Ganges and Brahmaputra rivers on their lower catchments (delta), did not change strongly during the Holocene and could not be responsible for the clay assemblage variations observed on sediments of the active levee.

Consequently, variations in the clay assemblage of the composite sediment record of the middle fan channel levee might reflect changes in the source area in the catchment basin of both rivers (highlands versus floodplain) and/or a modification of the weathering intensity conditions (pedogenesis) through the Holocene. Both of these processes could be driven by the changes of Indian summer monsoon rainfall.

4.4. Weathering History of the G-B River Catchment During the Holocene

Over the last decade, the dynamic of the Indian summer monsoon rainfall of the Holocene has been the focus of numerous studies based on (i) marine sediments of the Bay of Bengal [*Contreras-Rosales et al*., 2014; *Marzin et al*., 2013; *Zorzi et al*., 2015], (ii) lake sediments from North India [*Sarkar et al*., 2015], and (iii) speleothems from the Mawmluh Cave (northeast India) [*Berkelhammer et al*., 2012] and the Tibetan Plateau [*Gasse et al*., 1996; *Hong et al*., 2003]. We have reported in Figure 5, records from several sediment cores (Cores SO1888–342KL and MD77–176, Figure 1) retrieved in the northern Bay of Bengal [*Contreras-Rosales et al*., 2014; *Marzin et al*., 2013] for comparison with the smectite/(chlorite+illite) ratio record obtained herein. Ice-volume corrected alkane (n-C_{29} and n-C_{31}) hydrogen isotopic record (δDalk-ic) of Core SO188–342KL (19.9733°N, 90.0338°E, water depth 1265 m, Figure 1) has been shown to be strongly influenced by Indian summer monsoon rainfall [*Contreras-Rosales et al*., 2014]. An increase of the δDalk-ic corresponds to a decrease of summer monsoon rainfalls since heavy rainfalls are associated with negative δD values [*Contreras-Rosales et al*., 2014]. Past local $\delta^{18}O_w$ variations estimated from foraminifera assemblage-SSTs and $\delta^{18}O$ of the planktonic foraminifera *G. ruber* in Core MD77–176 (14°31′N, 93°08′E; water depth 1375 m, Figure 1) reflect freshwater discharges from the G-B river system and the Irrawaddy River [*Marzin et al*., 2013]. A decrease (increase) of the $\delta^{18}O_w$ indicates an increased (decreased) contribution of runoff and direct precipitation on the oxygen isotopic composition of surface water and, therefore, enhanced (weakened) Indian summer monsoon rainfalls. The stable carbon isotopic composition of leaf waxes (δ^{13}Cwax) from a core collected in the Lonar Lake (19°58′N, 76°30′E, Figure 1) [*Sarkar et al*., 2015] has been also reported in Figure 5. It provides information about vegetation composition in relation to environmental moisture/aridity [*Vogts et al*., 2012]. $\delta^{13}C$ values of long chain n-alkanes changes in vegetation (e.g., C_3 trees/C_4 grasses) can be detected [*Sinninghe Damsté et al*., 2011], since δ^{13}Cwax values clearly differ between C_3 and C_4 plants [*Rommerskirchen et al*., 2006; *Tipple and Pagani*, 2010] due to differences in carbon assimilation pathways

[*Eglinton and Eglinton*, 2008]. An increase of δ^{13}Cwax values indicates a change from predominantly woody C_3 (wetter climate) to C_4 grasses (drier climate) vegetation.

All these records indicate that the interval between 9.8 and 7 cal ka BP, characterized by low smectite/(illite+chlorite) ratios in our sedimentary record, corresponds to an interval of enhanced summer monsoon rainfall, triggering increased erosion of the highland of the G-B river basin. Thereafter this early Holocene wet interval, a gradual increase in the smectite/(illite+chlorite) ratio documents a progressive decrease of the summer monsoon rainfall, punctuated by more arid periods, as previously observed in Indian monsoon rainfall records reported in Figure 5 as well as in several other studies [e.g., *Gasse et al*., 1991, 1996; *Hong et al*., 2003; *Contreras-Rosales et al*., 2014; *Sarkar et al*., 2015; *Zorzi et al*., 2015]. More precisely, the smectite/(illite+chlorite) ratio distinctively increases between 5.0 and 4.0 cal ka BP, while the turbidite activity decreases [*Fournier et al*., 2016]. Such pattern highlights a drier phase during that time interval which is in total agreement with the previous climate reconstructions based on C_4 plant abundance and evaporites occurrence from sediment cores of the Lonar lake, which identified a peak of aridity between roughly 4.8 and 4 cal ka BP (Figure 5) [*Sarkar et al*., 2015]. This aridity peak is also well observed in the δ^{13}Cwax records and in a lesser extent by a decrease of the δDalk-ic record of Core SO 1888–342KL from the northern Bay of Bengal (Figure 5) [*Contreras-Rosales et al*., 2014].

This suggests that smectite/(illite+chlorite) ratio variations in sediments from the active levee system are likely linked to the Indian summer monsoon rainfall intensity during the Holocene. Wetter (drier) conditions are associated with significantly lower (higher) smectite/(illite+chlorite) ratios suggesting an increase of the relative contribution of clays from the highland of the G-B river basin compared to Indo-Gangetic plain one at the outlet of the G-B river system.

To reconstruct the evolution of chemical weathering in the Himalayan system (Himalayan ranges and Indo-Gangetic floodplain) the degree of weathering of the sediments has been documented using ratios of mobile to immobile elements such as K/Si following recent methodology proposed by *Lupker et al*. [2013]. The mineralogy of sediments from G-B river system is generally dominated by quartz, mica, and feldspars with occurrences of other phyllosilicates and clay minerals [*Galy et al*., 1996; *Garzanti et al*., 2011b]. These minerals are segregated during sediment transport on land [*Garzanti et al*., 2011b; *Lupker et al*., 2013] and by oceanic currents and gravity flow in the ocean [*Lupker et al*., 2013; *Joussain et al*., 2016] leading to a strong contrast in element ratios. For rivers samples, variations in terms of mineralogy and geochemistry are present through the water column. Because of progressive enrichment in slow-settling phyllosilicates toward the surface, elements mostly hosted in micas or associated with clays are generally concentrated in surface load (Al, Fe, Mg, K, Ti, P, Mn. . .). On the other hand, because of progressive enrichment in fast-settling coarser, denser elements which are mostly hosted in tectosilicates (Si, Na, Ca, and Sr), they are concentrated in deep load [*Garzanti et al*., 2011b].

As Al, Si, and Fe are not notably affected by chemical weathering during the Himalayan erosion, Al/Si and Fe/Si variability across the Indo-Gangetic plain as well as on shelf and Bengal Fan mainly represents a balance between quartz rich sediments (low Al/Si and Fe/Si ratios) and clay-rich sediments (high Al/Si and Fe/Si ratios) (Figure 4a) [*Galy and France-Lanord*, 2001; *Singh and France-Lanord*, 2002; *Lupker et al*., 2013].

Lupker et al. [2012] showed that mineral sorting is the first-order control on the major chemical composition of the G-B river sediments. They showed that taking into account this control, sediments become significantly depleted in mobile elements such as K during their transit from the highlands of the Himalayas to the Indo-Gangetic plain. In order to correct chemical compositions for bias induced by sediment sorting during transport, and to assess the degree of sediment weathering, *Lupker et al*. [2013] introduced a normalization of mobile to immobile ratios, K/Si* ratio to a common Al/Si ratio (described in detail in *Lupker et al*. [2013]). This normalization permits to correct the K/Si ratio from the sorting effect. For this correction, it is considered that each sample is a mixing between a coarse-grained end-member and a fine-grained end-member with an average Al/Si composition of sediments of 0.23 [*Lupker et al*., 2011]. Thus, relative variations of the K/Si* are considered to only represent changes of the state of the chemical weathering.

A strong correlation between K/Si and Al/Si ratios have been obtained in our sedimentary record ($r^2 = 0.77$). After the normalization, the coefficient of correlation between K/Si* and Al/Si ratios decrease strongly ($r^2 = 0.58$), which means that the sediment sorting has been accounted and that K/Si* is not dependent from the grain-size. Thus, the K/Si* can be used to establish state of chemical weathering of sediment input

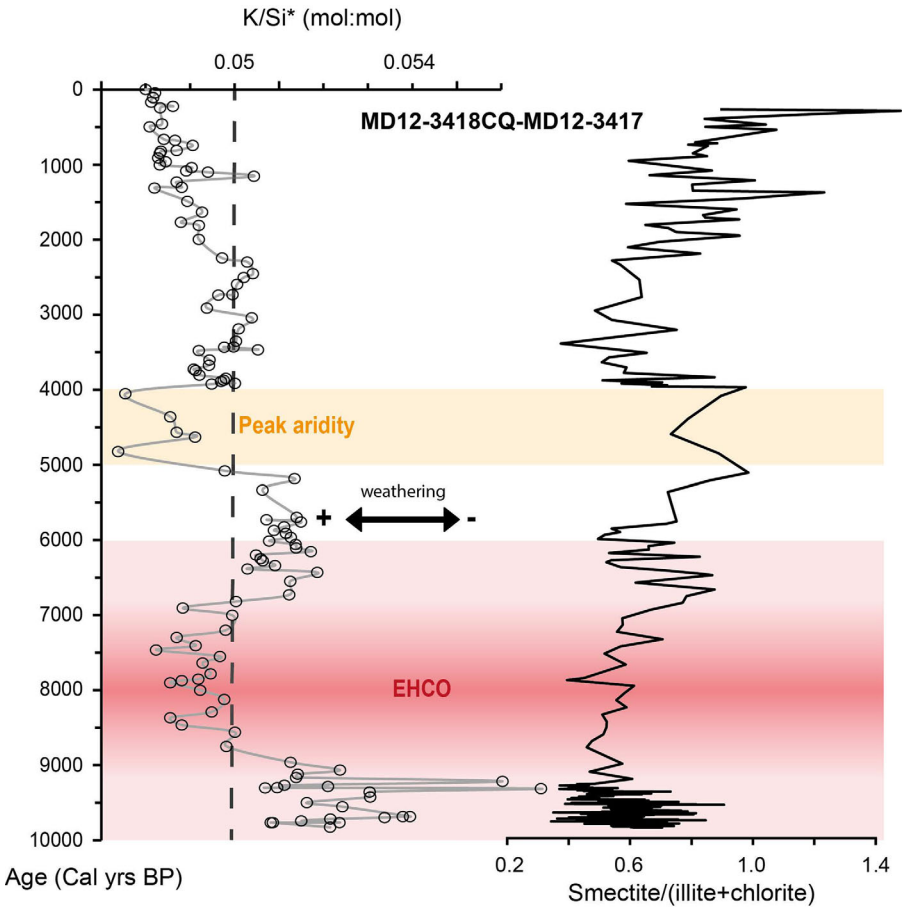

Figure 7. Evolution of K/Si* from sediments in the composite record for the last 10 cal ka BP. The Early Holocene Climatic Optimum (EHCO) are also displayed. The light orange box represents the aridity peak identified by *Sarkar et al.* [2015].

from the G-B river system as it was already done with success at a relatively low time resolution for Cores SO93–117KL, SO93–118KL, and SO93–120KL, located on the active levee [*Lupker et al.*, 2013]. K/Si* of our composite record has been reported in Figure 7. Its average value is ~0.050, and is slightly lower (0.052) than those obtained previously by *Lupker et al.* [2013] on sediments of the active levee for the Holocene. As turbidite layers are also not systematically associated with changes in K/Si* ratio, the sorting effect has been properly considered for this record.

In general, the K/Si* ratio displays a decreasing trend through the Holocene associated to an increasing of the smectite/(illite+chlorite) ratio. These long-term of K/Si* ratio variations could be associated to the reduction of the Indian monsoon rainfall that took place gradually since about 9.8 ka. In more detail, the time interval between 9.8 and 5 cal ka BP is characterized by higher K/Si* ratio ranging from 0.049 to 0.057 (Figure 7) interrupted by slightly lower ratio between 9.2 and 7 cal ka BP. This time interval is also associated to low smectite/(illite+chlorite) ratio (between 9.8 and 6 cal ka BP) indicating a strong contribution of clay minerals derived from the physical erosion of Himalaya's high reliefs. We infer that heavy monsoon rainfall of the beginning of the Holocene (between 9.8 and 6 cal ka BP) is associated to strong physical erosion and rapid transfers of sediments from the highlands to the Bengal Fan. This suggests that storage of sediments on the plain should have remained relatively reduced, limiting the formation of smectite. The time interval between 9 and 7 ka associated to the maximum of Indian monsoon rainfall corresponding also to a slightly lower K/Si* ratio that could reflect an increase chemical weathering of coarse primary minerals as smectite remain in low proportion for this time interval. We can hypothesis that this period of maximum of monsoon rainfall is associated to a rapid transfer of sediments slightly weathered from high relief to the Bengal deep-sea fan. Pollen records obtained on sediments off the eastern Indian coast, showed a long term drying trend through the Holocene from 11.3 cal ka BP to present time [*Zorzi et al.*, 2015]. In that study, pollen

assemblages are mainly composed of humid type plants (e.g., mangroves and coastal forest) for the early and the middle Holocene (11.3 to about 4 cal ka BP). Such vegetation cover could have protected the Indo-Gangetic plain soils from physical erosion during the Early Holocene.

From 5 cal ka BP to present time, K/Si* ratio values are generally lower than 0.05 indicating a higher degree of chemical weathering of sediments compared to those of the early Holocene (0.049–0.058). It appears that the mid-Holocene aridity conditions are associated with a higher degree of chemical weathering of sediments brought by the G-B river system (lower K/Si* and higher smectite/(illite+chlorite) ratios). This implies a less efficient transfer of sediments from the high relief of the Himalayas to the Bengal Fan associated to a reduction of the continental runoff, a reduction of water discharges of the Ganges and Brahmaputra rivers and/or a diminution of the vegetation cover [*Zorzi et al*., 2015]. This would induce a reduction of detrital material derived from the high relief of the Himalayas, and a preferential reworking of material from soil of the Indo-Gangetic floodplain. Such processes will induce sediments input from the G-B river system to the northern Bengal Fan characterized by high degree of chemical weathering (lower K/Si* ratio) and higher smectite contents. For the last 2.5 cal, impact of anthropogenic activity cannot be excluded and could have affected the stability of soil from the plain area; the deforestation might have enhanced the transport of secondary minerals (e.g., smectite) from the alluvial and the coastal plain to the Bay of Bengal [*Fournier et al*., 2016].

Such results indicate that clay assemblage from sediments originated from the G-B river basin is very reactive to variations in the Indian summer monsoon intensity since ~9.2 cal ka BP, i.e., once the levee of the actual channel has been formed [*Weber et al*., 1997; *Fournier et al*., 2016]. Such rapid response of erosion and sediment transfer to Indian summer monsoon rainfall by large Asian River has also been observed in sediments from the southern South China Sea off the Mekong River mouth over the last 25,000 years [*Colin et al*., 2010]. This has been interpreted by a modification of the sedimentation processes within the Mekong Basin (changes of erosion area) rather than an immediate response of chemical weathering (pedogenesis) in the plains.

5. Conclusions

Clay minerals, major elements concentrations, and Sr and Nd isotopic compositions of detrital fraction were analyzed on a composite sediment record retrieved on the active middle fan channel levee of the northern Bengal Fan to reconstruct sedimentary sources and weathering state of detrital material derived from the G-B river system over the last ~9.8 ka.

1. The sediments from the active channel levee show similar $^{87}Sr/^{86}Sr$ and εNd isotopic signatures than those measured in the G-B river sediments, indicating that during the last 9.8 cal ka BP, the studied levee has been fed by detrital material from the G-B river system.
2. Even if the source is constant over the Holocene, the clay assemblage (well expressed by the smectite/(illite+chlorite) ratio) and the state of chemical weathering of sediments reconstructed from major elements (well documented by the K/Si* index) reveal an important variability over the course of the Holocene.
3. The different phases of the levee's construction (and changing turbiditic activity), as well as modifications that occurred in the delta (e.g., migration of the river courses), did not significantly affect the smectite/(illite+chlorite) ratios. Modifications of the sources within the G-B catchment basin (highlands versus floodplain) and/or changes of weathering conditions control clay mineralogy and K/Si* of the sediments.
4. The smectite/(illite+chlorite) and K/Si* ratios suggest an increasing input of detrital material from the highlands (reliefs) during the early-middle Holocene (9.8–6 cal ka BP). These sediments did not experience an important chemical weathering (low smectite/(illite+chlorite) and high K/Si* values). To the opposite, during more arid periods (especially since 4 cal ka BP), material originated from the Indo-Gangetic plain became predominant as shown by the higher smectite content of our sedimentary record, suggesting a weakening of the summer monsoon and a decrease of rainfalls on the highlands. These sediments derived from Indo-Gangetic plain soils are Himalayan material previously deposited and altered (lower K/Si* ratio). Over the latest part of the Holocene (last 2.5 cal ka BP), the human activity (deforestation for agriculture) was likely responsible for the destabilization of soils in the plains, which enhanced their erosion and transport to the Bengal Fan.

5. Finally, our results indicate a rapid response of erosion and sediment transfer of the G-B river system to changes in both the continental vegetation types and the dynamic of the summer monsoon rainfall.

Acknowledgments
We especially thank Louise Bordier for her assistance in Sr and Nd isotopic composition measurements. This work was supported by the Labex L-IPSL (ANR-10-LABX-0018) and the MONOPOL ANR project (ANR 2011 Blanc SIMI 5–6 024 04). Ronan Joussain also thanks the China Scholarship Council for its financial support during his studies in China. All data can be found in Table 1 and in supporting information.

References

Ahmad, S. M., V. M. Padmakumari, and G. A. Babu (2009), Strontium and neodymium isotopic compositions in sediments from Godavari, Krishna and Pennar rivers, *Curr. Sci.*, *97*(12), 1766–1769.

Berkelhammer, M., A. Sinha, L. Stott, H. Cheng, F. Pausata, and K. Yoshimura (2012), An abrupt shift in the Indian monsoon 4000 years ago, in *Climates, Landscapes, and Civilizations*, edited by L. Giosan et al., pp. 75–88, AGU, Washington, D. C.

Bouquillon, A., H. Chamley, and F. Fröhlich (1989), Sédimentation argileuse au Cénozoïque supérieur dans l'Océan Indien nord-oriental, *Oceanol. Acta*, *12*(3), 133–147.

Bouquillon, A., C. France-Lanord, A. Michard, and J.-J. Tiercelin (1990), Sedimentology and isotopic chemistry of the Bengal Fan sediments: The denudation of the Himalaya, in *Proceedings of the Ocean Drilling Program, Scientific Results*, vol. 116, pp. 43–58, Ocean Drill. Program, College Station, Tex.

Cai, Y., H. Zhang, H. Cheng, Z. An, R. Lawrence Edwards, X. Wang, L. Tan, F. Liang, J. Wang, and M. Kelly (2012), The Holocene Indian monsoon variability over the southern Tibetan Plateau and its teleconnections, *Earth Planet. Sci. Lett.*, *335–336*, 135–144, doi:10.1016/j.epsl.2012.04.035.

Chauhan, O. S., and E. Vogelsang (2006), Climate induced changes in the circulation and dispersal patterns of the fluvial sources during late Quaternary in the middle Bengal Fan, *J. Earth Syst. Sci.*, *115*, 379–386.

Clemens, S. C., and W. L. Prell (1991), Late Quaternary forcing of Indian Ocean summer-monsoon winds: A comparison of Fourier model and general circulation model results, *J. Geophys. Res.*, *96*, 22,683–22,700.

Clemens, S. C., and W. L. Prell (2003), A 350,000 year summer-monsoon multi-proxy stack from the Owen Ridge, Northern Arabian Sea, *Mar. Geol.*, *201*, 35–51.

Colin, C., L. Turpin, J. Bertaux, A. Desprairies, and C. Kissel (1999), Erosional history of the Himalayan and Burman ranges during the last two glacial-interglacial cycles, *Earth Planet. Sci. Lett.*, *171*, 647–660.

Colin, C., L. Turpin, D. Blamart, N. Frank, C. Kissel, and S. Duchamp (2006), Evolution of weathering patterns in the Indo-Burman Ranges over the last 280 kyr: Effects of sediment provenance on 87Sr/86Sr ratios tracer, *Geochem. Geophys. Geosyst.*, *7*, Q03007, doi:10.1029/2005GC000962.

Colin, C., G. Siani, M.-A. Sicre, and Z. Liu (2010), Impact of the East Asian monsoon rainfall changes on the erosion of the Mekong River basin over the past 25,000 yr, *Mar. Geol.*, *271*, 84–92.

Contreras-Rosales, L. A., T. Jennerjahn, T. Tharammal, V. Meyer, A. Lückge, A. Paul, and E. Schefuß (2014), Evolution of the Indian Summer Monsoon and terrestrial vegetation in the Bengal region during the past 18 ka, *Quat. Sci. Rev.*, *102*, 133–148, doi:10.1016/j.quascirev.2014.08.010.

Copard, K., C. Colin, E. Douville, A. Freiwald, G. Gudmundsson, B. De Mol, and N. Frank (2010), Nd isotopes in deep-sea corals in the North-eastern Atlantic, *Quat. Sci. Rev.*, *29*, 2499–2508.

Curray, J. R., and D. G. Moore (1971), Growth of the Bengal deep-sea Fan and denudation in the Himalayas, *Geol. Soc. Am. Bull.*, *82*, 563–572.

Curray, J. R., F. J. Emmel, and D. G. Moore (2003), The Bengal Fan: Morphology, geometry, stratigraphy, history and processes, *Mar. Pet. Geol.*, *19*, 1191–1223.

Derry, L. A., and C. France-Lanord (1996), Neogene Himalayan weathering history and river $^{87}Sr/^{86}Sr$: Impact on the marine Sr record, *Earth Planet. Sci. Lett.*, *142*, 59–74.

Dykoski, C. A., R. L. Edwards, H. Cheng, D. Yuan, Y. Cai, M. Zhang, Y. Lin, J. Qing, Z. An, and J. Revenaugh (2005), A high-resolution, absolute-dated Holocene and deglacial Asian monsoon record from Dongge Cave, China, *Earth Planet. Sci. Lett.*, *233*, 71–86, doi:10.1016/j.epsl.2005.01.036.

Eglinton, T. I., and G. Eglinton (2008), Molecular proxies of paleoclimatology, *Earth Planet. Sci. Lett.*, *275*, 1–16.

Emmel, F. J., and J. R. Curray (1984), The Bengal Submarine Fan, Northeastern Indian Ocean, *Geo-Mar. Lett.*, *3*, 119–124.

Fagel, N., P. Debrabant, and L. André (1994), Clay supplies in the Central Indian Basin since the late Miocene: Climatic or tectonic control?, *Mar. Geol.*, *122*, 151–172.

Fagel, N., L. André, and P. Debrebant (1997), Multiple seawater-derived geochemical signatures in Indian oceanic pelagic clays, *Geochim. Cosmochim. Acta*, *61*(5), 989–1008.

France-Lanord, C., and L. A. Derry (1997), Organic carbon burial forcing of the carbon cycle from Himalayan erosion, *Nature*, *390*, 65–67.

France-Lanord, C., L. A. Derry, and A. Michard (1993), Evolution of the Himalaya since Miocene time: Isotopic and sedimentological evidence from the Bengal Fan, *Himalayan Tectonics*, *74*, 603–621.

Fontugne, M. R., and J.-C. Duplessy (1986), Variations of the monsoon regime during the upper Quaternary: Evidence from carbon isotopic record of organic matter in north Indian Ocean sediment cores, *Palaeogeogr. Palaeoclimatol. Palaeoecol.*, *56*, 69–88.

Fournier, L., K. Fauquembergue, S. Zaragosi, C. Zorzi, B. Malaizé, F. Bassinot, R. Joussain, C. Colin, E. Moreno, and F. Leparmentier (2016), The Bengal Fan: External controls on the Holocene Active Channel turbidite activity, *Holocene*, *27*(6), 900–913.

Galy, A., and C. France-Lanord (1999), Weathering processes in the Ganges–Brahmaputra basin and the riverine alkalinity budget, *Chem. Geol.*, *159*, 31–60.

Galy, A., and C. France-Lanord (2001), Higher erosion rates in the Himalaya: Geochemical constraints on riverine fluxes, *Geology*, *29*, 23–26.

Galy, A., C. France-Lanord, and L. A. Derry (1996), The Late Oligocene-Early Miocene Himalayan belt constraints deduced from isotopic compositions of Early Miocene turbidites in the Bengal Fan, *Tectonophysics*, *260*, 109–118.

Galy, A., C. France-Lanord, and L. A. Derry (1999), The strontium isotopic budget of Himalayan Rivers in Nepal and Bangladesh, *Geochim. Cosmochim. Acta*, *63*(13/14), 1905–1925.

Garzanti, E., S. Andò, C. France-Lanord, G. Vezzoli, P. Censi, V. Galy, and Y. Najman (2011a), Mineralogical and chemical variability of fluvial sediments 1. Bedload sand (Ganges–Brahmaputra, Bangladesh), *Earth Planet. Sci. Lett.*, *299*, 368–381.

Garzanti, E., S. Andò, C. France-Lanord, P. Censi, P. Vignola, V. Galy, and M. Lupker (2011b), Mineralogical and chemical variability of fluvial sediments 2. Suspended-load silt (Ganges–Brahmaputra, Bangladesh), *Earth Planet. Sci. Lett.*, *302*, 107–120.

Gasse, F., et al. (1991), A 13,000-year climate record from western Tibet, *Nature*, *353*, 742–745.

Gasse, F., E. Van Campo, and K. Wei (1996), Holocene environmental changes in Bangong Co basin (Western Tibet). Part 4: Discussion and conclusions, *Palaeogeogr. Palaeoclimatol. Palaeoecol.*, *120*, 79–92.
Gibbs, R. J. (1977), Clay mineral segregation in the marine environment, *J. Sediment. Petrol.*, *47*, 237–243.
Goldstein, S. J., and S. B. Jacobsen (1988), Nd and Sr isotopic systematic of river water suspended material: Implications for crustal evolution, *Earth Planet. Sci. Lett.*, *87*, 215–221.
Goodbred, S. L., and S. A. Kuehl (2000), The significance of large sediment supply, active tectonism, and eustasy on margin sequence development: Late Quaternary stratigraphy and evolution of the Ganges–Brahmaputra delta, *Sediment. Geol.*, *133*, 227–248, doi:10.1016/S0037-0738(00)00041-5.
Goodbred, S. L., P. M. Paolo, M. S. Ullah, R. D. Pate, S. R. Khan, S. A. Kuehl, S. K. Singh, and W. Rahaman (2014), Piecing together the Ganges-Brahmaputra-Meghna River delta: Use of sediment provenance to reconstruct the history and interaction of multiple fluvial systems during Holocene delta evolution, *Geol. Soc. Am. Bull.*, *126*, 1495–1510.
Grant, K., E. Rohling, M. Bar-Matthews, A. Ayalon, M. Medina-Elizalde, C. B. Ramsey, C. Satow, and A. Roberts (2012), Rapid coupling between ice volume and polar temperature over the past 150,000 years, *Nature*, *491*, 744–747.
Holtzapffel, T. (1985), *Les Minéraux Argileux: Préparation, Analyse Diffractométrique et Détermination*, vol. 12, 136 pp., Société Géologique du Nord Publ.
Hong, Y. T., et al. (2003), Correlation between Indian Ocean summer monsoon and North Atlantic climate during the Holocene, *Earth Planet. Sci. Lett.*, *211*, 371–380.
Huyghe, P., R. Guilbaud, M. Bernet, A. Galy, A. P. Gajurel (2011), Significance of the clay mineral distribution in fluvial sediments of the Neogene to Recent Himalayan Foreland Basin (west-central Nepal), *Basin Res.*, *23*, 332–345, doi:10.1111/j.1365-2117.2010.00485.x.
Islam, M. S., and M. J. Tooley (1999), Coastal and sea-level changes during the Holocene in Bangladesh, *Quat. Int.*, *55*, 61–75, doi:10.1016/S1040-6182(98)00025-1.
Jacobsen, S. B., and G. J. Wasserburg (1980), Sm-Nd isotopic evolution of chondrites, *Earth Planet. Sci. Lett.*, *50*(1), 139–155.
Joussain R., C. Colin, Z. Liu, L. Meynadier, L. Fournier, K. Fauquembergue, S. Zaragosi, F. Schmidt, V. Rojas, and F. Bassinot (2016), Climatic control of sediment transport from the Himalayas to the proximal NE Bengal Fan during the last glacial-interglacial cycle, *Quat. Sci. Rev.*, *148*, 1–16, doi:10.1016/j.quascirev.2016.06.016.
Kudrass, H. R., A. Hofmann, H. Doose, K. Emeis, and H. Erlenkeuser (2001), Modulation and amplification of climatic changes in the Northern Hemisphere by the Indian summer monsoon during the past 80 ky, *Geology*, *29*(1), 63–66.
Licht, A., C. France-Lanord, L. Reisberg, C. Fontaine, A. N. Soe, and J. J. Jaeger (2013), A palaeo Tibet–Myanmar connection? Reconstructing the Late Eocene drainage system of central Myanmar using a multi-proxy approach, *J. Geol. Soc.*, *170*, 929–939, doi:10.1144/jgs2012-126.
Liu, Z., C. Colin, A. Trentesaux, D. Blamart, F. Bassinot, G. Siani, and M. A. Sicre (2004), Erosional history of the eastern Tibetan Plateau since 190 kyr ago: Clay mineralogical and geochemical investigations from the southwestern South China Sea, *Mar. Geol.*, *209*, 1–18.
Liu, Z., C. Colin, A. Trentesaux, G. Siani, N. Frank, D. Blamart, and S. Farid (2005), Late Quaternary climatic control on erosion and weathering in the eastern Tibetan Plateau and the Mekong Basin, *Quat. Res.*, *63*, 316–328.
Liu, Z., et al. (2016), Source-to-Sink transport processes of fluvial sediments in the South China Sea, *Earth Sci. Rev.*, *153*, 238–273.
Liu, Z. F., and X. J. Li (2011), Discussion on smectite formation in South China Sea sediments [in Chinese with English abstract], *Quat. Sci.*, *31*, 199–206.
Liu, Z. F., et al. (2010), Clay mineral distribution in surface sediments of the northeastern South China Sea and surrounding fluvial drainage basins: Source and transport, *Mar. Geol.*, *277*, 48–60.
Lugmair, G. W., T. Shimamura, R. S. Lewis, and E. Anders (1983), Samarium-146 in the early solar system: Evidence from neodymium in the allende meteorite, *Science*, *222*, 1015–1018.
Lupker, M., C. France-Lanord, J. Lavé, J. Bouchez, V. Galy, F. Métivier, J. Gaillardet, B. Lartiges, J.-L. Mugnier (2011), A rouse-based method to integrate the chemical composition of river sediments: Application to the Ganga basin, *J. Geophys. Res.*, *116*, F04012, doi:10.1029/2010JF001947.
Lupker, M., C. France-Lanord, V. Galy, J. Lavé, J. Gaillardet, A. P. Gajurel, C. Guilmette, M. Rahman, S. K. Singh, and R. Sinha (2012), Predominant floodplain over mountain weathering of Himalayan sediments (Ganga basin), *Geochim. Cosmochim. Acta*, *84*, 410–432.
Lupker, M., C. France-Lanord, V. Galy, J. Lavé, and H. Kudrass (2013), Increasing chemical weathering in the Himalayan system since the Last Glacial Maximum, *Earth Planet. Sci. Lett.*, *365*, 243–252.
Marzin, C., N. Kallel, M. Kageyama, J.-C. Duplessy, and P. Braconnot (2013), Glacial fluctuations of the Indian monsoon and their relationship with North Atlantic climate: New data and modelling experiments, *Clim. Past*, *9*, 2135–2151.
Milliman, J. D., and R. H. Meade (1983), World-wide delivery of river sediment to the oceans, *J. Geol.*, *91*, 1–21.
Milliman, J. D., and J. P. M. Syvitski (1992), Geomorphic/tectonic control of sediment discharge to the ocean: The importance of small mountainous rivers, *J. Geol.*, *100*, 525–544.
Patchineelam, S. M., and A. M. De Figueiredo (2000), Preferential settling of smectite on the Amazon continental shelf, *Geo-Mar. Lett.*, *20*, 37–42.
Peng, Z. X., J. J. Mahoney, P. Hooper, C. Harris, and J. Beane (1994), A role for lower continental crust in flood basalt genesis? Isotopic and incompatible element study of the lower six formations of the western Deccan Traps, *Geochim. Cosmochim. Acta*, *57*, 5109–5130.
Petschick, R. (2000), MacDiff software. [Available at http://servermac.geologie.un-frankfurt.de/Rainer.html]
Pickering, J. L., S. L. Goodbred, M. D. Reitz, T. R. Hartzog, D. R. Mondal, and M. S. Hossain (2014), Late Quaternary sedimentary record and Holocene channel avulsions of the Jamuna and Old Brahmaputra River valleys in the upper Bengal delta plain, *Geomorphology*, *227*, 123–136.
Pierson-Wickmann, A.-C., L. Reisberg, C. France-Lanord, and H. R. Kudrass (2001), Os-Sr-Nd results from sediments in the Bay of Bengal: Implications for sediment transport and the marine Os record, *Paleoceanography*, *16*, 435–444.
Prell, W. L. (1984), Monsoonal climate of the Arabian Sea during the Late Quaternary: A response to changing solar radiation, in *Milankovitch and Climate*, edited by A. L. Berger et al., pp. 349–366, D. Riedel, Hingham, Mass.
Prell, W. L., and J. E. Kutzbach (1987), Monsoon variability over the past 150,000 years, *J. Geophys. Res.*, *92*(D7), 8411–8425.
Rashid, T., S. Suzuki, H. Sato, M. H. Monsur, and S. K. Saha (2013), Relative sea-level changes during the Holocene in Bangladesh, *J. Asian Earth Sci.*, *64*, 136–150.
Reimer, P. J., et al. (2013), INTCAL13 & MARINE13 radiocarbon calibration curves 0–50,000 years cal BP, *Radiocarbon*, *55*(4), 1869–1887.
Rommerskirchen, F., A. Plader, G. Eglinton, Y. Chikaraishi, and J. Rullkötter (2006), Chemotaxonomic significance of distribution and stable carbon isotopic composition of long-chain alkanes and alkan-1-ols in C4 grass waxes, *Org. Geochem.*, *37*, 1303–1332.
Sarin, M. M., S. Krishnaswanmi, K. Dilli, B. K. L. Somayajulu, and W. S. Moore (1989), Major ion chemistry of the Ganges-Brahmaputra river system: Weathering processes and fluxes to the Bay of Bengal, *Geochim. Cosmochim. Acta*, *53*, 997–1009.

Sarkar, A., R. Ramesh, S. K. Bhattacharya, and G. Rajagopalan (1990), Oxygen isotope evidence for a stronger winter monsoon current during the last glaciation, *Nature*, *348*, 549–551.
Sarkar, S., S. Prasad, H. Wilkes, N. Riedel, M. Stebich, N. Basavaiah, and D. Sachse (2015), Monsoon source shifts during the drying mid-Holocene: Biomarker isotope based evidence from the core "monsoon zone" (CMZ) of India, *Quat. Sci. Rev.*, *123*, 144–157.
Singh, S. K., and C. France-Lanord (2002), Tracing the distribution of erosion in the Brahmaputra watershed from isotopic compositions of stream sediments, *Earth Planet. Sci. Lett.*, *202*, 645–662.
Singh, M., I. B. Singh, and G. Müller (2007), Sediment characteristics and transportation dynamics of the Ganges River, *Geomorphology*, *86*, 144–175.
Singh, S. K., S. K. Rai, and S. Krishnaswami (2008), Sr and Nd isotopes in River sediments from the Ganges basin: Sediment provenance and spatial variability in physical erosion, *J. Geophys. Res.*, *113*, F03006, doi:10.1029/2007JF000909.
Sinninghe Damsté, J. S., D. Verschuren, J. Ossebaar, J. Blokker, R. van Houten, B. Plessen, and S. Schouten (2011), A 25,000-year record of climate-induced changes in lowland vegetation of eastern equatorial Africa revealed by the stable carbon-isotopic composition of fossil plant leaf waxes, *Earth Planet. Sci. Lett.*, *302*, 236–246.
Southon, J., M. Kashgarian, M. Fontugne, B. Metivier, and W. W.-S. Yim (2002), Marine reservoir corrections for the Indian Ocean and Southeast Asia, *Radiocarbon*, *44*, 167–180.
Stuiver, M., and P. J. Reimer (1993), Calib Users Guide Revision 3.0, Quat. Isotopes Lab., Univ. of Wash., Seattle.
Tanaka, T., et al. (2000), JNdi-1: A neodymium isotopic reference in consistency with La Jolla neodymium, *Chem. Geol.*, *168*, 279–281.
Tripathy, G. R., S. K. Singh, R. Bhushan, and V. Ramaswamy (2011), Sr-Nd isotope composition of the Bay of Bengal sediments: Impacts of Climate on Erosion of the Himalaya, *Geochem. J.*, *45*, 175–186.
Tripathy, G. R., S. K. Singh, and V. Ramaswamy (2014), Major and trace element geochemistry of Bay of Bengal sediments: Implications to provenances and their controlling factors, *Palaeogeogr. Palaeoclimatol. Palaeoecol.*, *397*, 20–30.
Tipple, B. J., and M. Pagani (2010), A 35 Myr North American leaf-wax compound-specific carbon and hydrogen isotope record: Implications for C_4 grasslands and hydrologic cycle dynamics, *Earth Planet. Sci. Lett.*, *299*, 250–262.
Umitsu, M. (1993), Late quaternary sedimentary environments and landforms in the Ganges Delta, *Sediment. Geol.*, *83*, 177–186.
Unger, D., V. Ittekkot, P. Schäfer, J. Tiemann, and S. Reschke (2003), Seasonality and interannual variability of particle fluxes to the deep Bay of Bengal: Influence of riverine input and oceanographic processes, *Deep Sea Res., Part II*, *50*, 897–923.
Vogts, A., E. Schefuß, T. Badewien, and J. Rullkötter (2012), *n*-Alkane parameters from a deep sea sediment transect off southwest Africa reflect continental vegetation and climate conditions, *Org. Geochem.*, *47*, 109–119.
Weber, M. E., M. H. Wiedicke, H. R. Kudrass, C. Hübscher, and H. Erlenkeuser (1997), Active growth of the Bengal Fan during sea-level rise and highstand, *Geology*, *25*, 315–318.
Webster, P. J. (1987), *The Elementary Monsoon*, pp. 3–32, John Wiley, New York.
Zorzi, C., M. F. Sanchez Goñi, K. Anupama, S. Prasad, V. Hanquiez, J. Johnson, and L. Giosan (2015), Indian monsoon variations during three contrasting climatic periods: The Holocene, Heinrich Stadial 2 and the last interglacial–glacial transition, *Quat. Sci. Rev.*, *125*, 50–60.